Research Square

Preprints are preliminary reports that have not undergone peer review.
They should not be considered conclusive, used to inform clinical practice,
or referenced by the media as validated information.

Structural Relationships, Petrographic Characteristics and Bulk Geochemistry of Chromite Mineralization in the Balıköy–Tavşanlı Ophiolitic Rocks, NW Türkiye

Taşkın Deniz Yıldız[1]

tdyildiz@atu.edu.tr

Adana Alparslan Türkeş Science and Technology University

Şenel Özdamar[2]

Istanbul Technical University

Article

Keywords: chromite mineralization, podiform chromitite, ophiolite, dunite, structural deformation, serpentinization, bulk XRF, Tavşanlı, northwestern Türkiye

Posted Date: November 6th, 2026

DOI: https://doi.org/10.21203/rs.3.rs-11403775/v1

License: This work is licensed under a Creative Commons Attribution 4.0 International License.
Read Full License

Additional Declarations: No competing interests reported.

Abstract

Chromitites hosted by ophiolitic ultramafic rocks record melt–rock interaction and mantle processes, yet their present-day geometry may be substantially modified by tectonic deformation and serpentinization. This study documents the Balıköy–Tavşanlı chromite occurrence in northwestern Türkiye through integrated field mapping, structural observations, petrography, ore microscopy and bulk X-ray fluorescence (XRF) geochemistry. The mineralization is hosted predominantly by variably serpentinized dunite and is concentrated in three approximately parallel NW–SE-trending zones that dip about 45° northwestward and broadly parallel the regional thrust architecture. Chromite occurs as disseminated, spotted/leopard, banded–lenticular and massive aggregates. Fracturing, fragmentation, brecciation and cataclastic textures are common, while the host-rock matrix contains serpentine, talc and locally secondary carbonate, albite and Fe-oxide phases. Nine bulk-ore samples contain 27.79–41.18 wt% Cr, 40.62–60.19 wt% Cr_2O_3 and 4.50–9.44 wt% Fe; reported Cr/Fe ratios range from 3.31 to 7.95. The spatial correspondence between mineralized zones and thrust-related structures documents a strong structural relationship, but does not demonstrate syn-thrust chromite formation. The most conservative interpretation is that deformation modified the present geometry and textures of pre-existing chromite-bearing bodies. The study provides a field-based framework for exploration while distinguishing observed surface relationships from unverified subsurface continuities and unresolved genetic interpretations.

1. Introduction

Podiform chromitites hosted by ophiolitic mantle sections are important records of melt migration, melt–peridotite interaction and the tectonomagmatic evolution of oceanic lithosphere. Their formation is commonly related to focused transport of chromite-saturated melts through peridotite, interaction between infiltrating melts and mantle rocks, and local accumulation of Cr-spinel in dunite-rich channels [1–4]. Recent syntheses emphasize that chromitites may preserve evidence of multiple stages of mantle evolution, although the relative importance of individual processes varies among localities and must be evaluated against the available petrographic and geochemical evidence [5–7].

The primary mineralogical and textural signatures of chromitite can be modified by processes operating after crystallization. Deformation during subduction, obduction, thrust stacking and later tectonic reactivation may fracture, dismember, displace or reorient chromitite bodies. Serpentinization and hydrothermal alteration can modify the ultramafic matrix and may also affect Cr-spinel margins or produce secondary Fe-bearing phases [2, 14–16, 24, 27]. Grain-scale deformation of chromite has been documented in other ophiolitic systems and may record mechanical modification after initial mineral formation [23]. Accordingly, the present geometry of a chromitite body should not automatically be equated with its primary magmatic geometry.

The Tethyan ophiolites provide a valuable framework for comparing chromitites formed in different mantle environments. Their mineralogical and compositional diversity, including variation in chromite

chemistry and platinum-group element (PGE) assemblages, underscores the need to distinguish field-scale similarities from mineral-chemical evidence for a shared petrogenesis [7]. In northwestern Türkiye, the Orhaneli–Harmancık–Tavşanlı region contains extensive ultramafic rocks and chromitite occurrences within the tectonic architecture of the İzmir–Ankara–Erzincan suture system. Previous studies have documented the geological setting, geochemistry and supra-subduction-related characteristics of the regional ophiolites, as well as the mineralogical, compositional and metasomatic histories of Orhaneli and Harmancık chromitites [8–13, 20–22, 25, 26]. These studies provide regional context but cannot substitute for deposit-scale observations at Balıköy.

The Balıköy occurrence lies within this regional ophiolitic framework and is characterized by chromite-bearing dunitic ultramafic rocks, pervasive deformation and variable serpentinization. Despite the substantial regional literature, an integrated deposit-scale description linking the local structural distribution, ore textures, host-rock alteration and bulk-ore chemistry is needed to characterize the exposed occurrence. A key question is whether the spatial coincidence between chromite-bearing zones and the thrust architecture records primary structural control on chromitite formation or later tectonic reorganization of pre-existing chromitite bodies.

Here, we document the field distribution, structural relationships, petrographic characteristics and bulk XRF composition of the Balıköy chromite mineralization. The specific objectives are to: (1) describe the geometry of mineralized zones and their relationship to the mapped structural fabric; (2) characterize the range of chromite textures and the deformation features preserved by the ore; (3) document the mineralogical variability and secondary alteration of the host rocks; and (4) evaluate the bulk Cr, Cr_2O_3, Fe and Cr/Fe data in the context of regional chromitite studies. Because the XRF measurements are bulk-ore analyses rather than in-situ Cr-spinel compositions, we do not calculate Cr# or Mg# or assign a definitive tectonomagmatic subtype on the basis of these data alone.

2. Geological Setting

The Balıköy area lies in northwestern Anatolia within the Tavşanlı Zone and the broader İzmir–Ankara–Erzincan suture system. The Tavşanlı Zone is commonly interpreted as the northern subducted margin of the Anatolide–Tauride Block and records Cretaceous high-pressure–low-temperature metamorphism followed by exhumation [17–19]. Its regional architecture includes metamorphic rocks, ophiolitic mélange and ophiolitic rocks assembled during the closure of Neo-Tethyan oceanic domains [18, 19, 26]. These relationships establish the tectonic setting in which the Balıköy ultramafic rocks are now exposed, but do not by themselves determine the age or origin of the local chromite mineralization. The regional location of the study area is shown in Fig. 1.

The Orhaneli–Harmancık–Tavşanlı ophiolitic belt includes dunite- and harzburgite-bearing peridotites, serpentinized ultramafic rocks, mafic dykes and ophiolitic mélange. Geochemical studies of the Harmancık ophiolite have identified characteristics consistent with a supra-subduction-zone setting [8, 20, 22], while mineralogical and compositional investigations of Orhaneli and Harmancık chromitites

have emphasized melt–peridotite interaction, chromitite formation, and later metasomatic or hydrothermal modification [9–13, 21, 25]. More recent work on the Bursa ophiolite continues to refine relationships among mantle-hosted podiform chromitites, crust–mantle transition-zone chromitites and evolving forearc melts [12, 26]. These regional interpretations provide context for Balıköy; they are not direct evidence that the local mineralization shares every inferred genetic feature.

Figure 1. Regional geological and tectonic setting of the Balıköy–Tavşanlı study area. (a) Major tectonic zones and ophiolitic belts of Türkiye and northwestern Anatolia; (b) location of Balıköy within the Orhaneli–Harmancık–Tavşanlı ophiolitic belt. Modified and redrawn from Okay [18], Manav et al. [8] and Uysal et al. [9].

The study area covers approximately 3.25 km² and is dominated by peridotitic–dunitic ultramafic rocks, with ophiolitic mélange, local diabase dykes, Neogene cover deposits and recent alluvium. The ultramafic rocks are variably serpentinized, fractured and locally strongly deformed. Chromite occurs mainly within dunitic rocks. The mapped lithologies, structural elements, former workings, GPS stations and sample locations are shown in Fig. 2. Representative field exposures of the host rocks, chromite occurrences, serpentine schist and altered ultramafic rocks are illustrated in Fig. 4.

Figure 2. Geological and structural map of the Balıköy study area at 1:10,000 scale, showing ultramafic rocks, structural elements, chromite occurrences, former workings and sample locations.

The A–A' section shows the dominance of peridotitic rocks, local diabase dykes and the mapped thrust relationship (Fig. 3). Cr-bearing zones drawn beneath the surface represent interpreted continuations, not drilling-confirmed ore bodies. They are therefore treated as exploration hypotheses rather than demonstrated three-dimensional continuities.

Figure 3. A–A' geological cross-section showing peridotitic rocks, local diabase dykes, observed and interpreted Cr-bearing zones, and the thrust relationship. Subsurface Cr-bearing geometries are interpretive.

Figure 4. Representative field views of peridotitic host rocks, Cr-bearing zones, serpentine schist and altered ultramafic rocks.

3. Methods

3.1. Field mapping and structural measurements

Detailed geological mapping was conducted at 1:10,000 scale over approximately 3.25 km². Lithological contacts, alteration, faults and fractures, former pits and trenches, exposed mineralization and structural orientations were recorded. Twenty-seven GPS stations were examined and 23 field samples were collected. Mineralized structures were measured where exposure permitted. Three approximately parallel NW–SE-trending mineralized zones were recognized, generally dipping about 45° northwestward.

The geological map integrates lithological boundaries, structural elements, old workings, GPS locations and sampling sites (Fig. 2).

Because many historical workings are closed or partly covered, directly exposed mineralization was distinguished from loose chromite fragments and other indicators around abandoned workings. This distinction is important: isolated fragments and historical workings can guide exploration, but neither alone establishes continuous ore at depth. Field sketches of selected workings and exposures are shown in Fig. 5, while additional field photographs document the mineralization and its relationship to altered host rocks (Fig. 6).

3.2. Petrography and ore microscopy

Twenty-eight samples were examined for host-rock mineralogy, serpentinization, secondary mineral development and chromite textures. Particular attention was given to fracturing, fragmentation, brecciation and cataclastic deformation of chromite and to serpentine, talc, calcite, albite and secondary Fe-oxide phases. Selected ore samples were examined by reflected-light ore microscopy. Representative transmitted-light petrographic textures are shown in Fig. 7, and ore-microscopic features are illustrated in Fig. 8. Modal estimates are retained as observational values; differences among source records were not artificially reconciled.

3.3. Geochemical analysis

Nine chromite-ore samples were ground to < 0.074 mm and dried at 105°C for 3 h before bulk XRF analysis. Elemental Cr and Fe, Cr_2O_3 and Cr/Fe were evaluated. The source analytical table also reports FeO, Fe_2O_3 and $FeCr_2O_4$, plus one incompletely defined derived parameter; only unambiguous elemental Cr, Cr_2O_3, Fe and Cr/Fe are used here. The full values retained from the detailed analytical table are presented in Table 2 and visualized in Fig. 9. Because these are bulk-ore data, they are not interpreted as individual Cr-spinel compositions and are not used to derive Cr# or Mg#.

4. Results

4.1. Structural distribution of the mineralization

Chromite mineralization is hosted mainly by variably serpentinized dunite. The ultramafic rocks are commonly fractured, crushed and deformed. Chromite indicators are not evenly distributed but cluster within three approximately parallel NW–SE-trending zones (Fig. 2). These zones generally dip about 45° northwestward and broadly parallel the regional thrust orientation. At one directly exposed locality, a massive chromite-rich zone approximately 20–30 cm thick dips about 45° northwestward. The A–A' section summarizes the observed structural relationships and separates exposed Cr-bearing zones from interpreted subsurface continuations (Fig. 3).

Figure 5. Selected field sketches of former workings and chromite-bearing exposures. (a) Former working in fractured dunite; (b) mineralized trench in serpentinized dunite; (c) directly observed

approximately 20–30 cm-thick massive chromite zone; (d) mineralized pit near the thrust trace.

Figure 6. Representative field views of chromite mineralization and former workings, including mineralized zones, banded chromite and altered host rocks.

4.2. Ore textures and deformation

Chromite occurs as disseminated, spotted/leopard, banded–lenticular and massive aggregates. Disseminated chromite is commonly fine grained and dispersed through serpentinized dunite, whereas chromite-rich material develops spotted, banded, lenticular and massive fabrics. Microscopically, chromite grains commonly show fracturing, fragmentation, brecciation and cataclastic deformation. Sample 4 contains fragmented chromite within a deformed, oriented serpentine-rich fabric; sample 7 contains fragmented chromite with secondary calcite and albite; sample 8 is strongly fractured and cataclastic; and sample 19 contains chromite fragments in a breccia with serpentine and secondary carbonate (Fig. 7).

Figure 7. Petrographic features of chromite-bearing rocks. (a) Fragmented chromite in a deformed, oriented serpentine-rich fabric; (b) cataclastic chromite with secondary calcite and albite; (c) chromite-rich cataclastic texture with serpentine and talc; (d) brecciated chromite with secondary carbonate and serpentine. Image width: 3.5 mm.

Ore microscopy confirms variable deformation intensity (Fig. 8). Sample 8 contains fragmented and locally crushed/mylonitic chromite; sample 14 contains coarse fractured and brecciated grains; sample 22A shows a rim-like texture described in the source record as magnetitization; and sample 23 contains abundant, strongly fractured chromite with local crushing or mylonitization. The description “magnetitization” is retained as a source observation and is not treated as mineral-chemical confirmation of magnetite.

Figure 8. Ore-microscopic characteristics of selected chromite ores. (a) Fragmented and crushed/mylonitic chromite; (b) coarse fractured and brecciated chromite; (c) rim-like texture described as magnetitization in the source record; (d) strongly fractured and locally crushed/mylonitized chromite.

4.3. Petrography and secondary mineral development

The ultramafic host rocks are variably to strongly serpentinized. Serpentine-group minerals dominate many matrices, with local talc, secondary calcite and albite. Opaque Fe-oxide phases occur locally. Chromite abundance varies strongly from disseminated grains in serpentinized matrix to chromite-rich rocks dominated by fractured and brecciated chromite. Representative sample-level modal descriptions are summarized in Table 1, while the textural context of selected specimens is shown in Figs. 7 and 8.

Table 1
Representative petrographic characteristics and modal estimates. Values are observational estimates and were not reconciled where source records differed. Sample 23 has differing source estimates and should be treated as approximate.

Sample Nr.	Texture	Chromite / opaque phase	Secondary minerals
4	Deformed, oriented, cataclastic	40–45% chromite	55–60% serpentine; chrysotile, antigorite, talc
6A	Deformed, carbonate–clayey	40–42% chromite	Calcite + clay + talc matrix
7	Cataclastic, fragmented	40–45% chromite	50–55% calcite; 5–6% albite
8	Chromite-rich, cataclastic	65–70% chromite	30–35% serpentine + talc
15B	Strongly serpentinized, mesh	7–8% chromite + Fe oxides	92–93% serpentine
19	Brecciated chromite	65–70% chromite	Calcite + serpentine matrix
20	Deformed, oriented mesh	15–18% chromite; 2–3% Fe oxides	79–85% serpentine
21A	Deformed mesh	7–8% chromite; 9–10% Fe oxides	82–85% serpentine
22A	Strongly serpentinized	10–12% chromite; 3–4% Fe oxides	54–62% serpentine; 25–30% talc
23	Chromite-rich, deformed	75–80% chromite*	Serpentinized matrix

Table 1. Representative petrographic characteristics and modal estimates. Values are observational estimates and were not reconciled where source records differed. Sample 23 has differing source estimates and should be treated as approximate.

4.4. Bulk-ore geochemistry

Nine bulk XRF analyses yield 27.79–41.18 wt% Cr, 40.62–60.19 wt% Cr_2O_3, 4.50–9.44 wt% Fe and reported Cr/Fe ratios of 3.31–7.95 (Table 2; Fig. 9). The reported mean values are 34.49 wt% Cr, approximately 50.33 wt% Cr_2O_3, approximately 7.84 wt% Fe and approximately 4.51 for Cr/Fe. Sample 22 has the highest Cr and Cr_2O_3 concentrations, sample 18 the lowest Cr concentration, and sample 16 the highest reported Cr/Fe ratio and lowest Fe concentration. These are bulk-composition differences and should not be interpreted as direct measurements of individual chromite-grain composition.

Table 2
Bulk XRF composition of chromite-ore samples. The Cr/Fe value of 4.07 for sample 20 is retained from the detailed source table; the discrepancy with the summary table and the ratio calculated directly from the displayed Cr and Fe values should be checked against the original laboratory record.

Sample	Cr wt%	Cr_2O_3 wt%	Fe wt%	Cr/Fe
5	31.28	45.72	9.44	3.31
15	32.60	47.65	9.41	3.46
16	35.79	52.31	4.50	7.95
18	27.79	40.62	6.69	4.15
19	29.01	42.40	8.41	3.45
20	34.85	50.93	8.49	4.07
21	34.05	49.76	7.43	4.58
22	41.18	60.19	8.04	5.12
23	36.53	53.39	8.15	4.48

Table 2. Bulk XRF composition of chromite-ore samples. The Cr/Fe value of 4.07 for sample 20 is retained from the detailed source table; the discrepancy with the summary table and the ratio calculated directly from the displayed Cr and Fe values should be checked against the original laboratory record.

Figure 9. Geochemical characteristics of the chromite ores: (a) elemental Cr; (b) Cr_2O_3; (c) Fe; and (d) reported Cr/Fe ratios.

5. Discussion

The integrated observations indicate that the present geometry of the Balıköy chromite occurrence is strongly influenced by structural reworking, although the relative timing of mineralization and deformation is not directly constrained. Three observations are central: the concentration of mineralization along NW–SE-trending zones broadly parallel to the thrust architecture; the widespread fracturing, brecciation and cataclastic deformation of chromite; and the variable serpentinization and secondary mineral development in the host dunite (Figs. 2–8). Taken together, these observations establish a strong relationship between the current distribution of chromite-bearing rocks and the structural/alteration history of the host rocks.

Importantly, spatial coincidence with the thrust system does not demonstrate that chromitite formed during thrusting. Podiform chromitites are generally linked to melt migration, melt–peridotite reaction and local chromite saturation in mantle environments [1–4]. Recent syntheses also emphasize that

chromitites can preserve multi-stage records, but such models require mineralogical, textural and geochemical evidence appropriate to each locality [5–7]. The Balıköy dataset contains no direct age constraint linking chromite formation to thrusting and no mineral-scale chemical data capable of resolving a specific primary tectonomagmatic environment. In contrast, fractured, brecciated and locally crushed fabrics are consistent with mechanical modification of already consolidated chromitite bodies. The most conservative interpretation is therefore that the present thrust architecture influenced the distribution, segmentation or exposure of pre-existing mineralization rather than that it generated the chromite itself.

This interpretation is compatible with the regional setting but does not depend on transferring a regional genetic model directly to Balıköy. Orhaneli and Harmancık chromitites have been interpreted in relation to supra-subduction-zone mantle processes, melt–rock interaction and compositional variation [8–13, 20–22, 25, 26]. Work on the Bursa ophiolite further highlights the possibility of linked processes in mantle peridotites and the crust–mantle transition zone [12]. These studies are useful comparators, but the present Balıköy dataset does not include in-situ Cr-spinel major- and trace-element chemistry, PGE data or mineral-scale redox measurements. Consequently, a definitive classification as a particular chromitite subtype or a claim of direct genetic equivalence with a nearby occurrence would exceed the available evidence.

The petrographic assemblage records both mechanical deformation and alteration. Serpentinization is widespread, while talc, carbonate, albite and Fe-oxide phases occur locally (Table 1; Figs. 7–8). Natural and experimental studies show that serpentinization and hydrothermal alteration can affect Cr-spinel margins, textures and local chemistry [14–16, 24, 27]. The rim-like feature described as magnetitization in sample 22A may be consistent with secondary modification, but its mineralogical identity and chemical composition have not been verified by electron-probe microanalysis or SEM–EDS. No specific reaction pathway or fluid condition is therefore assigned to this feature. The current observations support a history of alteration but do not resolve the number, timing or physicochemical conditions of alteration episodes.

The bulk XRF results demonstrate sample-scale chemical heterogeneity (Table 2; Fig. 9). The reported Cr_2O_3 range of 40.62–60.19 wt% and Cr/Fe range of 3.31–7.95 document substantial chromium enrichment in the analyzed material. However, bulk chemistry is controlled not only by the composition of chromite but also by the proportion of chromite relative to silicate matrix and secondary phases. Sample 16, for example, has the highest reported Cr/Fe ratio and the lowest Fe concentration; its ratio should not be read as an independent mineral-chemical indicator of tectonic setting. Chromite petrogenesis in regional and global studies is commonly evaluated using in-situ Cr-spinel composition, including Cr#, Mg#, TiO_2 and trace elements, together with inclusions and PGE systematics [3, 7, 9–11, 13, 15, 21, 22, 25]. Those data are not available for Balıköy, so no such parameters or classifications are inferred here.

From an exploration perspective, the three NW–SE corridors are priority surface-based targets because they combine mapped structural alignment, exposed chromite occurrences and former workings (Figs. 2, 3, 5 and 6). Nevertheless, the subsurface geometries shown in Fig. 3 remain interpretive. The current dataset does not demonstrate three-dimensional continuity, tonnage, grade continuity or an economic resource. Follow-up work should first refine structural mapping and sample representativeness, then use suitable geophysical methods and drilling to test the inferred geometry and construct a three-dimensional geological model. In parallel, EPMA or SEM–EDS analyses, chromite trace-element measurements and PGE studies would provide the mineral-specific constraints needed to distinguish primary chromitite signatures from later alteration. Such work is required before the economic significance of the Balıköy occurrence can be evaluated.

More broadly, Balıköy demonstrates why structural architecture must be separated from genetic interpretation in deformed ophiolitic chromitite systems. A mineralized zone may be aligned with structures visible today even if the chromitite formed earlier. Combining map-scale geometry (Figs. 2–3), field-scale exposures (Figs. 4–6), petrographic and ore-microscopic textures (Figs. 7–8), and bulk chemistry (Table 2; Fig. 9) provides a more robust basis for describing the present state of the occurrence. The main contribution is therefore a deposit-scale observational framework and a transparent statement of what the current dataset can—and cannot—resolve.

5.1. Structural organization versus primary chromitite geometry

The mapped NW–SE-trending corridors are a robust feature of the exposed occurrence, but the data resolve their present orientation more clearly than their original geometry. A primary magmatic lens can be displaced or fragmented during later tectonic assembly, and structurally aligned fragments can produce a map pattern that resembles primary continuity. Conversely, structures may localize exposure or preserve mineralized rocks without having controlled the initial segregation of chromite. The available map and section (Figs. 2–3) show spatial correspondence, whereas the field sketches and photographs (Figs. 5–6) document only selected accessible exposures. Because parts of the old workings are covered or inaccessible and the subsurface projections have not been tested by drilling, continuity between separate exposures remains an interpretation. The manuscript therefore treats the three corridors as mapped or inferred structural–mineralization trends, not as proven continuous ore shoots.

5.2. What the deformation textures do and do not establish?

Fracturing, fragmentation, brecciation and cataclastic textures in chromite-bearing samples (Figs. 7–8) provide direct evidence for mechanical disruption. Their occurrence alongside fractured and deformed host ultramafic rocks supports post-crystallization or late-stage deformation of the mineralized assemblage. However, these textures alone do not uniquely identify the deformation environment, pressure–temperature conditions, shear sense or age. The term “mylonitic” is retained only where it

occurs in the source descriptions; a rigorous diagnosis of crystal-plastic deformation would require microstructural criteria and, ideally, crystallographic or electron-microscopy observations. Likewise, the spatial association with a thrust cannot be used as a temporal tie unless cross-cutting relations or independent geochronological constraints establish that relationship. This distinction is consistent with structural studies of chromite-bearing ophiolites, where ore-body geometry and grain-scale deformation are evaluated together rather than treating either as a stand-alone genetic indicator [23, 28].

5.3. Alteration overprint and mineralogical uncertainty

The contrast between chromite-rich specimens and strongly serpentinized samples (Table 1) indicates that the studied material encompasses a range of ore-to-matrix proportions and alteration intensities. Serpentine, talc, calcite, albite and opaque Fe-bearing phases occur in different combinations. These assemblages are consistent with modification of ultramafic rocks after their initial formation, but they do not define a unique alteration sequence. In particular, the source description of a rim-like “magnetitization” texture in sample 22A should be treated as a petrographic observation rather than a confirmed mineral-chemical identification. Cr-spinel may be modified during serpentinization and hydrothermal activity, as reported from other ophiolitic systems [14–16, 24, 27], yet the degree and mechanism of modification at Balıköy cannot be established without grain-scale chemical data. Future analyses should target chromite cores and rims, adjacent opaque phases, and the immediate silicate matrix, so that primary compositions can be distinguished from secondary reaction products.

5.4. Regional comparison and limits of tectonomagmatic inference

Regional studies of the Orhaneli and Harmancık ophiolites provide a useful comparison because they document chromitites associated with dunite, melt–rock interaction, and supra-subduction-related geochemical signatures [8–13, 20–22, 25, 26]. Studies of the broader Tethyan belt also demonstrate that chromitite composition and PGE assemblages can vary considerably between localities and ore types [3, 7, 15]. However, the Balıköy dataset comprises bulk XRF data and petrographic observations, not in-situ analyses of Cr-spinel. Therefore, the regional literature supports the geological plausibility of interpreting Balıköy within an ophiolitic chromitite system, but it does not justify transferring a specific parental-melt composition or tectonic subtype to this occurrence. Establishing such a comparison would require electron-probe analyses of chromite (including Cr_2O_3, Al_2O_3, MgO, FeO/Fe_2O_3 and TiO_2), trace-element measurements, and, where appropriate, PGE and inclusion studies. Recent work on the Bursa ophiolite illustrates how such mineral-specific and stratigraphic/structural data can refine links between mantle-hosted and crust–mantle transition-zone chromitites [12].

5.5. Bulk chemistry and exploration significance

The bulk XRF dataset (Table 2; Fig. 9) demonstrates that the nine analyzed samples are chromium-rich but compositionally variable. Bulk Cr and Cr_2O_3 values depend on the amount of chromite in the analyzed material as well as the composition of the non-ore matrix; Fe may be contributed by chromite, silicates and secondary opaque phases. As a result, these values are appropriate for describing the analyzed

specimens but cannot independently reveal chromite-grain chemistry, parental melt characteristics or deposit-scale grade continuity. The three corridors, the observed 20–30 cm-thick massive zone, and the locations of former workings provide practical targets for follow-up mapping. They do not establish a resource or reserve. A defensible exploration model requires representative channel sampling, systematic mapping of orientation and thickness, suitable geophysical surveys, drilling, QA/QC documentation and three-dimensional modelling. Resource statements should be avoided until those data are available.

5.6. Study contribution and priorities for future work

The main contribution of this study is the integration of local structural mapping, field-scale ore occurrence, petrographic and ore-microscopic observations, and bulk XRF results into one explicitly constrained description of Balıköy. The integrated evidence suggests that the present distribution of chromite is structurally organized and that deformation and serpentinization have modified the exposed mineralized rocks. It does not resolve the original age of chromite formation, the exact chronology of deformation and alteration, or the three-dimensional extent of the mineralization. The most valuable next steps are therefore: (i) systematic structural measurements and oriented sampling across all three corridors; (ii) mineral-chemical analyses of chromite cores, rims and associated opaque phases; (iii) representative bulk sampling with analytical quality control; (iv) trace-element and PGE characterization where justified; and (v) geophysical surveys and drilling to test the interpreted subsurface geometry. These investigations would allow the local occurrence to be compared more rigorously with regional chromitites and would provide the evidence needed for a meaningful assessment of exploration potential.

The regional comparison above draws on the published work on chromitite formation and modification [1–7], Harmancık and Orhaneli ophiolite geology and geochemistry [8–13, 20–22, 25, 26], serpentinization and hydrothermal overprinting [14–16, 24, 27], the Tavşanlı Zone and sub-ophiolite setting [17–19], and structural deformation of chromite-bearing bodies [23, 28]. These references are used as comparative context; none substitutes for mineral-chemical or subsurface evidence from Balıköy itself.

Conclusions

Chromite mineralization at Balıköy is hosted mainly by variably serpentinized dunite and is concentrated in three approximately parallel NW–SE-trending zones dipping about 45° northwestward (Figs. 2–3).

The spatial parallelism between mineralized zones and the thrust architecture establishes a strong structural relationship but does not prove syn-thrust chromitite formation. The observed fractured, brecciated and cataclastic textures are consistent with later mechanical modification of pre-existing chromite-bearing bodies (Figs. 5–8).

Disseminated, spotted/leopard, banded–lenticular and massive chromite textures coexist. Petrographic observations document variable serpentinization, talc formation and local secondary carbonate, albite and Fe-oxide phases (Table 1; Figs. 7–8).

Serpentinization, talc formation and local secondary carbonate, albite and Fe-oxide development demonstrate substantial post-formational alteration. The exact nature of the apparent magnetite-rich rims requires mineral-chemical verification.

Bulk XRF analyses yield 27.79–41.18 wt% Cr, 40.62–60.19 wt% Cr_2O_3, 4.50–9.44 wt% Fe and reported Cr/Fe ratios of 3.31–7.95 (Table 2; Fig. 9). These data characterize the analyzed bulk samples and cannot replace individual Cr-spinel mineral chemistry.

The three NW–SE mineralized corridors provide priority exploration targets, but their subsurface continuity and economic significance remain unproven. Detailed structural mapping, representative sampling, geophysics, drilling, three-dimensional modelling and mineral-chemical characterization are required to evaluate the occurrence further (Figs. 2–3).

Declarations

Competing Interests

The authors declare no competing interests.

Funding

The authors received no specific funding for this work.

Author Contribution

T.D.Y. conceived and designed the study, integrated and interpreted the field, petrographic and geochemical data, prepared the figures and tables, and drafted the manuscript. Ş.Ö. contributed to the field studies, geological interpretation and evaluation of the results. Both authors reviewed and approved the final manuscript.

Acknowledgement

We would like to thank Prof. Dr. Bektaş Uz for his valuable contributions to the fieldwork.

Data Availability

All data generated or analysed during this study are included in this published article and its Supplementary Information.

References

1. Arai, S. Origin of podiform chromitites. *J. Asian Earth Sci.* **15**, 303–310. https://doi.org/10.1016/S0743-9547(97)00015-9 (1997).
2. Arai, S. & Miura, M. Formation and modification of chromitites in the mantle. *Lithos* **264**, 277–295. https://doi.org/10.1016/j.lithos.2016.08.039 (2016).
3. González-Jiménez, J. M. et al. Chromitites in ophiolites: How, where, when, why? Part II. The crystallization of chromitites. *Lithos* **189**, 140–158. https://doi.org/10.1016/j.lithos.2013.09.008 (2014).
4. Payot, B. D., Arai, S., Tamayo, R. A. Jr. & Yumul, G. P. Jr. Textural evidence for the chromite-oversaturated character of the melt involved in podiform chromitite formation. *Resour. Geol.* **63**, 313–319. https://doi.org/10.1111/rge.12011 (2013).
5. Xiong, F. et al. Podiform chromitites as multi-stage mantle archives: Integrating deep-mantle inheritance with shallow mantle processes. *Earth-Sci. Rev.* **281**, 105605. https://doi.org/10.1016/j.earscirev.2026.105605 (2026).
6. Aslan, L. & Üner, T. Cr-spinel compositions and the petrogenesis of podiform chromitites in the Kağızman Ophiolite (Ağrı, Eastern Türkiye). *Geol. Carpath.* **77**, 275–289. https://doi.org/10.31577/GeolCarp.2026.14 (2026).
7. Zaccarini, F., Economou-Eliopoulos, M., Tsikouras, B. & Garuti, G. Chromite composition and platinum-group elements distribution in Tethyan chromitites of the Mediterranean Basin: An overview. *Minerals* **14**, 744. https://doi.org/10.3390/min14080744 (2024).
8. Manav, H., Gültekin, A. H. & Uz, B. Geochemical evidence for the tectonic setting of the Harmancık ophiolites, NW Turkey. *J. Asian Earth Sci.* **24**, 1–9. https://doi.org/10.1016/S1367-9120(03)00018-X (2004).
9. Uysal, İ. et al. Genesis and geodynamic significance of chromitites from the Orhaneli and Harmancık ophiolites (Bursa, NW Turkey) as evidenced by mineralogical and compositional data. *Ore Geol. Rev.* **65**, 26–41. https://doi.org/10.1016/j.oregeorev.2014.08.006 (2015).
10. Akbulut, M. et al. A record of metasomatism and crustal contamination of the Mediterranean lithosphere in chromitites of the Orhaneli Ophiolite Complex (NW Türkiye). *J. Asian Earth Sci.* **236**, 105311. https://doi.org/10.1016/j.jseaes.2022.105311 (2022).
11. Arslan, E. et al. Geochemistry of mantle peridotites and chromitites from Upper Cretaceous ophiolites in NW Türkiye: Insights into abyssal to forearc mantle settings. *Lithos* **514–515** https://doi.org/10.1016/j.lithos.2025.108208 (2025).
12. Gao, P. et al. Genesis of chromitites from the mantle and crust–mantle transition zone: Constraints from the Bursa Ophiolite, NW Turkey. *Acta Geol. Sin Engl. Ed.* **100**, 1063–1085.

https://doi.org/10.1111/1755-6724.70086 (2026).

13. Chen, C. et al. Formation process of dunites and chromitites in Orhaneli and Harmancık ophiolites (NW Turkey): Evidence from in-situ Li isotopes and trace elements in olivine. *Lithos* **376–377**, 105773. https://doi.org/10.1016/j.lithos.2020.105773 (2020).
14. Eslami, A., Malvoisin, B. & Brunet, F. Hydrothermal alteration of chromitite-dunite pairs from the Sabzevar ophiolite (NE Iran): Chemical and nano-textural evolution of Cr-spinel. *Lithos* **442–443**, 107093. https://doi.org/10.1016/j.lithos.2023.107093 (2023).
15. Liu, R., Zhao, J. H., Zhou, M. & Qi, H. Alteration of chromite during serpentinization of peridotites. *Lithos* **460–461**, 107385. https://doi.org/10.1016/j.lithos.2023.107385 (2023).
16. Liu, X. et al. Post-magmatic hydrothermal activities in the Bursa ophiolite (NW Turkey): Implications for unusual minerals recovered from ophiolites. *Lithos* **436–437**, 106957. https://doi.org/10.1016/j.lithos.2022.106957 (2023).
17. Önen, A. P. & Hall, R. Sub-ophiolite metamorphic rocks from NW Anatolia, Turkey. *J. Metamorph Geol.* **18**, 483–495. https://doi.org/10.1046/j.1525-1314.2000.00276.x (2000).
18. Okay, A. I. & Tavşanlı, Z. The northern subducted margin of the Anatolide-Tauride Block. *Bull. Min. Res. Explor.* **142**, 191–221 (2011).
19. Özdamar, Ş. et al. Metamorphism, magmatism, and exhumation history of the Tavşanlı Zone, NW Turkey: New petrological constraints. *Turk. J. Earth Sci.* **27**, 269–293. https://doi.org/10.3906/yer-1712-14 (2018).
20. Bacak, G. & Uz, B. Dağardı güneyi Tavşanlı Kütahya ofiyolitinin jeolojisi ve jeokimyasal özellikleri. *İTÜ Dergisi/D Mühendislik*. **2**, 86–98 (2003).
21. Sarıfakıoğlu, E., Özen, H. & Winchester, J. A. Whole rock and mineral chemistry of ultramafic-mafic cumulates from the Orhaneli (Bursa) Ophiolite, NW Anatolia. *Turk. J. Earth Sci.* **18**, 55–83. https://doi.org/10.3906/yer-0806-8 (2009).
22. Sarıfakıoğlu, E., Özen, H., Çolakoğlu, A. & Sayak, H. Petrology, mineral chemistry, and tectonomagmatic evolution of Late Cretaceous suprasubduction-zone ophiolites in the İzmir–Ankara–Erzincan suture zone, Turkey. *Int. Geol. Rev.* **52**, 187–222. https://doi.org/10.1080/00206810902818479 (2010).
23. Ghosh, B., Ray, J. & Morishita, T. Grain-scale plastic deformation of chromite from podiform chromitite of the Naga-Manipur ophiolite belt, India: Implication to mantle dynamics. *Ore Geol. Rev.* **56**, 199–208. https://doi.org/10.1016/j.oregeorev.2013.09.001 (2014).
24. Su, B. X. et al. The occurrence, origin, and fate of water in chromitites in ophiolites. *Am. Mineral.* **105**, 894–903. https://doi.org/10.2138/am-2020-7270 (2020).
25. Akmaz, R. M., Uysal, İ. & Saka, S. Compositional variations of chromite and solid inclusions in ophiolitic chromitites from southeastern Turkey: Implications for chromitite genesis. *Ore Geol. Rev.* **58**, 208–224. https://doi.org/10.1016/j.oregeorev.2013.11.007 (2014).
26. Xin, G. et al. Subduction initiation in the Neo-Tethys and formation of the Bursa ophiolite in NW Turkey. *Lithos* **422–423**, 106746. https://doi.org/10.1016/j.lithos.2022.106746 (2022).

27. Chen, C., Wang, C. Y., Yang, S. & Uysal, İ. Hydrothermal origin of platinum-group minerals during serpentinization of the podiform chromitites from the Kızıldağ ophiolite in southern Türkiye. *Chem. Geol.* **674**, 122563. https://doi.org/10.1016/j.chemgeo.2024.122563 (2025).
28. Rassios, A. et al. A structural approach to the genesis of chrome ores within the Vourinos ophiolite (Greece). *Ore Geol. Rev.* **125**, 103684. https://doi.org/10.1016/j.oregeorev.2020.103684 (2020).

Figures

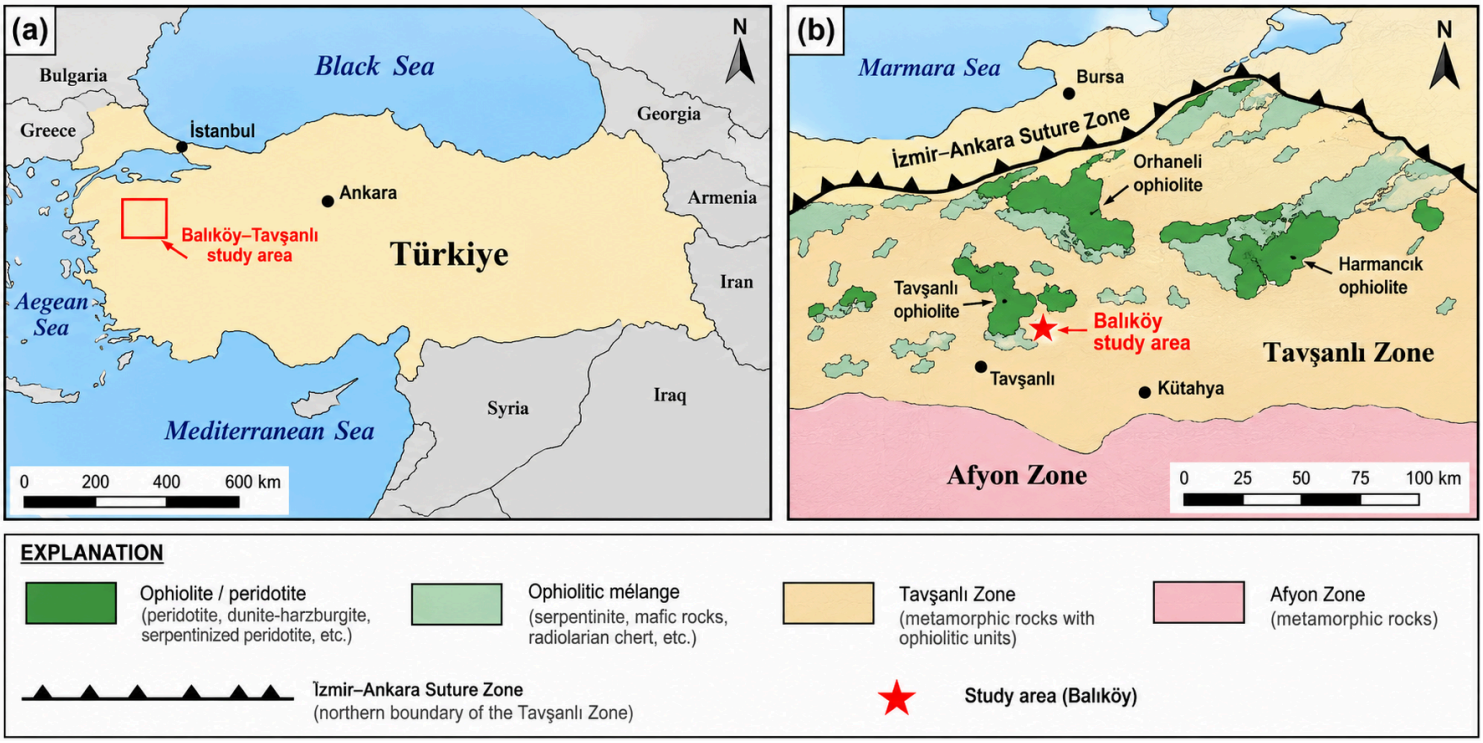


Figure 1

Regional geological and tectonic setting of the Balıköy–Tavşanlı study area. (a) Major tectonic zones and ophiolitic belts of Türkiye and northwestern Anatolia; (b) location of Balıköy within the Orhaneli–Harmancık–Tavşanlı ophiolitic belt. Modified and redrawn from Okay [18], Manav et al. [8] and Uysal et al. [9].

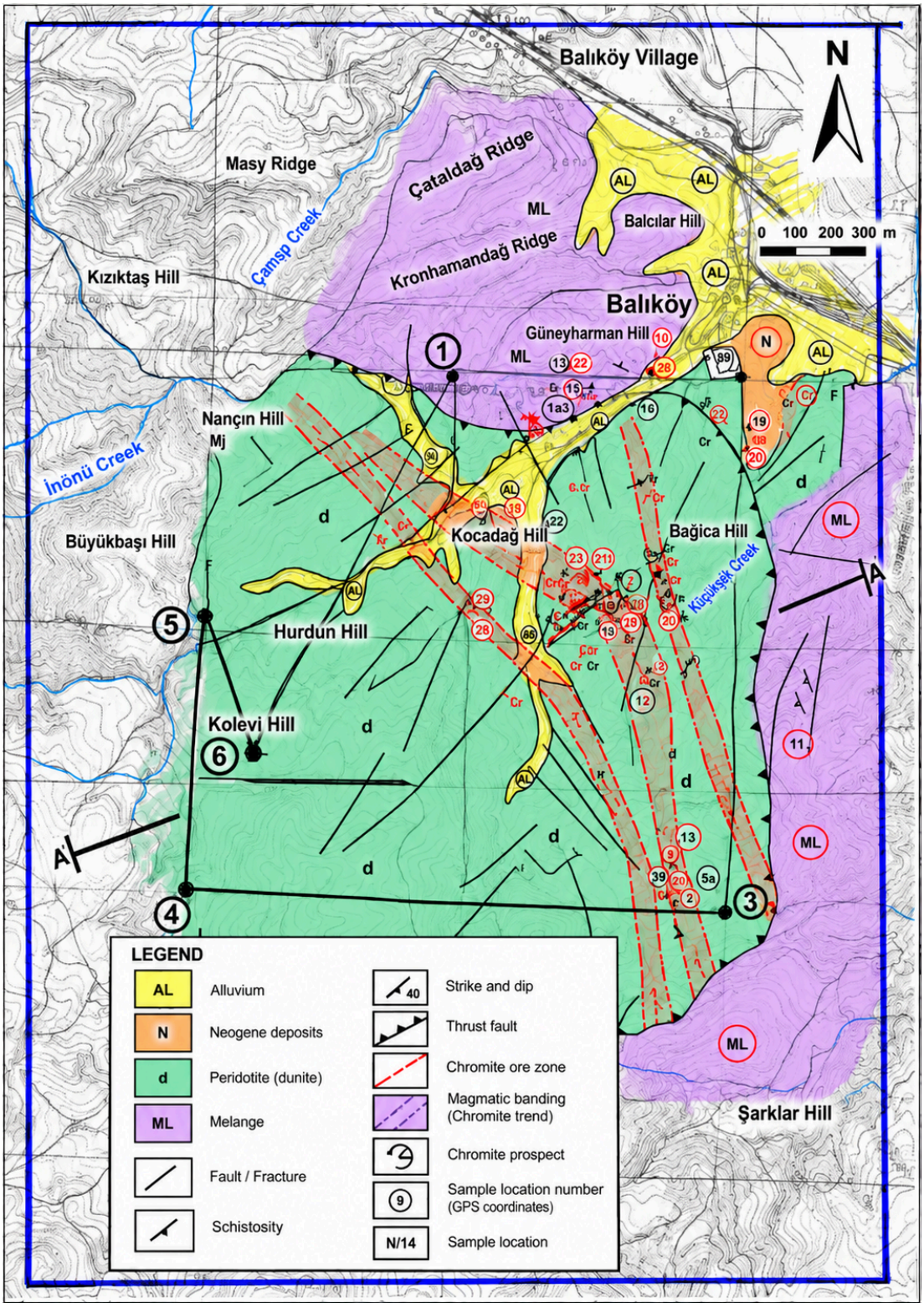


Figure 2

Geological and structural map of the Balıköy study area at 1:10,000 scale, showing ultramafic rocks, structural elements, chromite occurrences, former workings and sample locations.

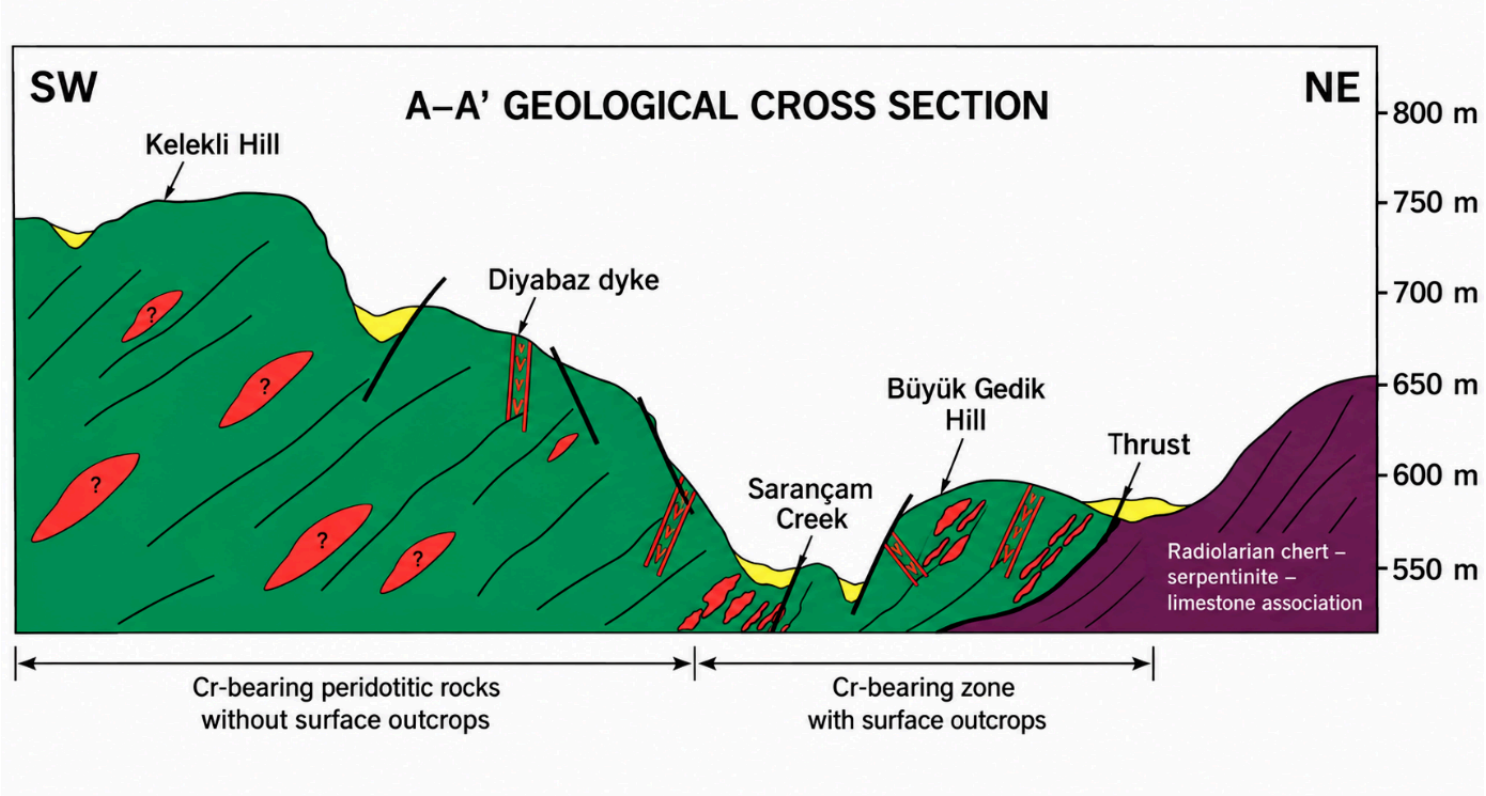


Figure 3

A–A' geological cross-section showing peridotitic rocks, local diabase dykes, observed and interpreted Cr-bearing zones, and the thrust relationship. Subsurface Cr-bearing geometries are interpretive.

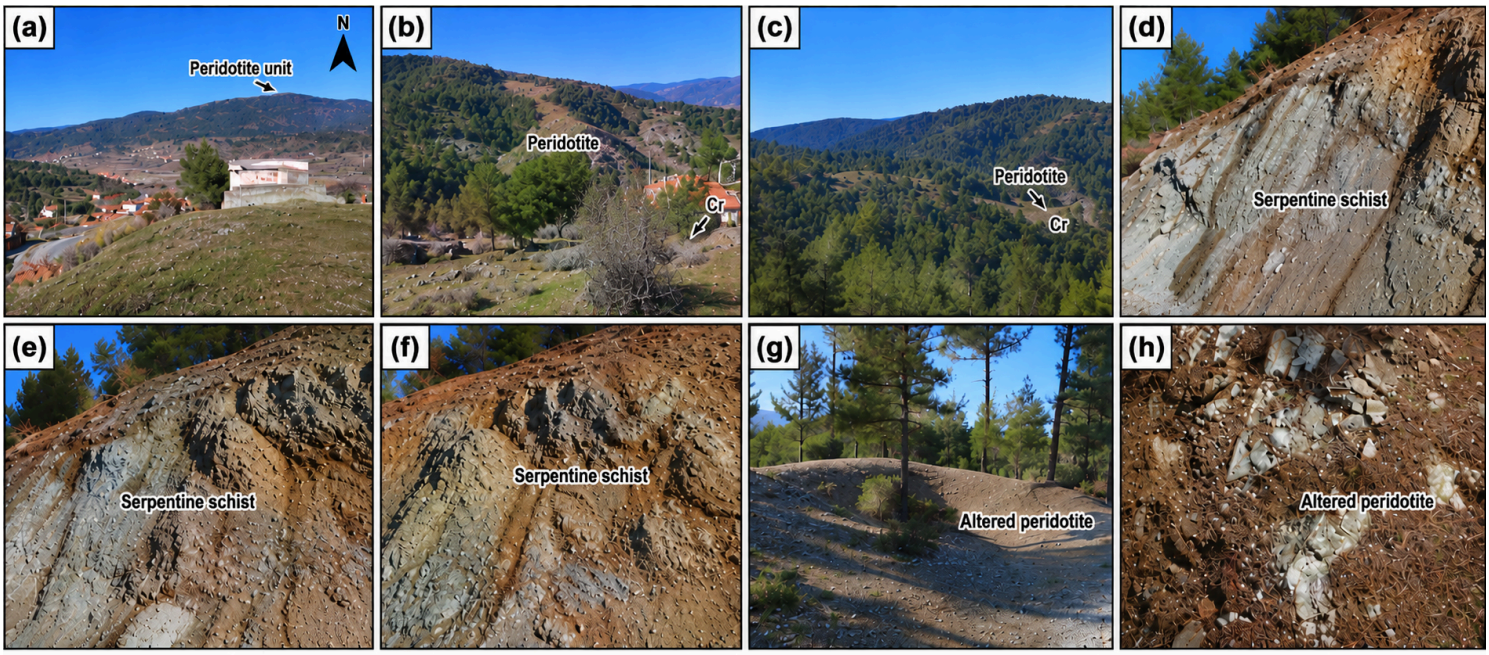


Figure 4

Representative field views of peridotitic host rocks, Cr-bearing zones, serpentine schist and altered ultramafic rocks.

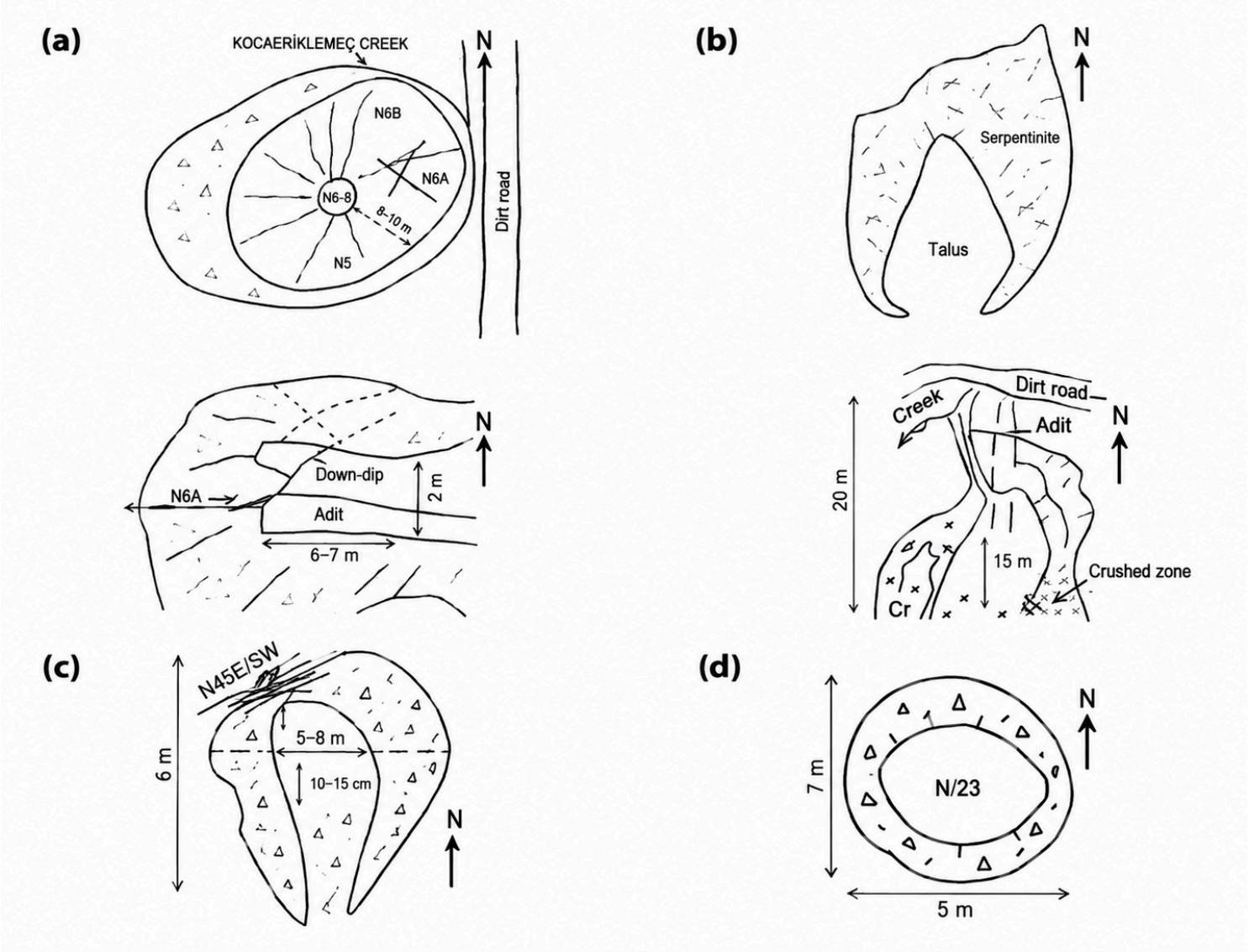


Figure 5

Selected field sketches of former workings and chromite-bearing exposures. (a) Former working in fractured dunite; (b) mineralized trench in serpentinized dunite; (c) directly observed approximately 20–30 cm-thick massive chromite zone; (d) mineralized pit near the thrust trace.

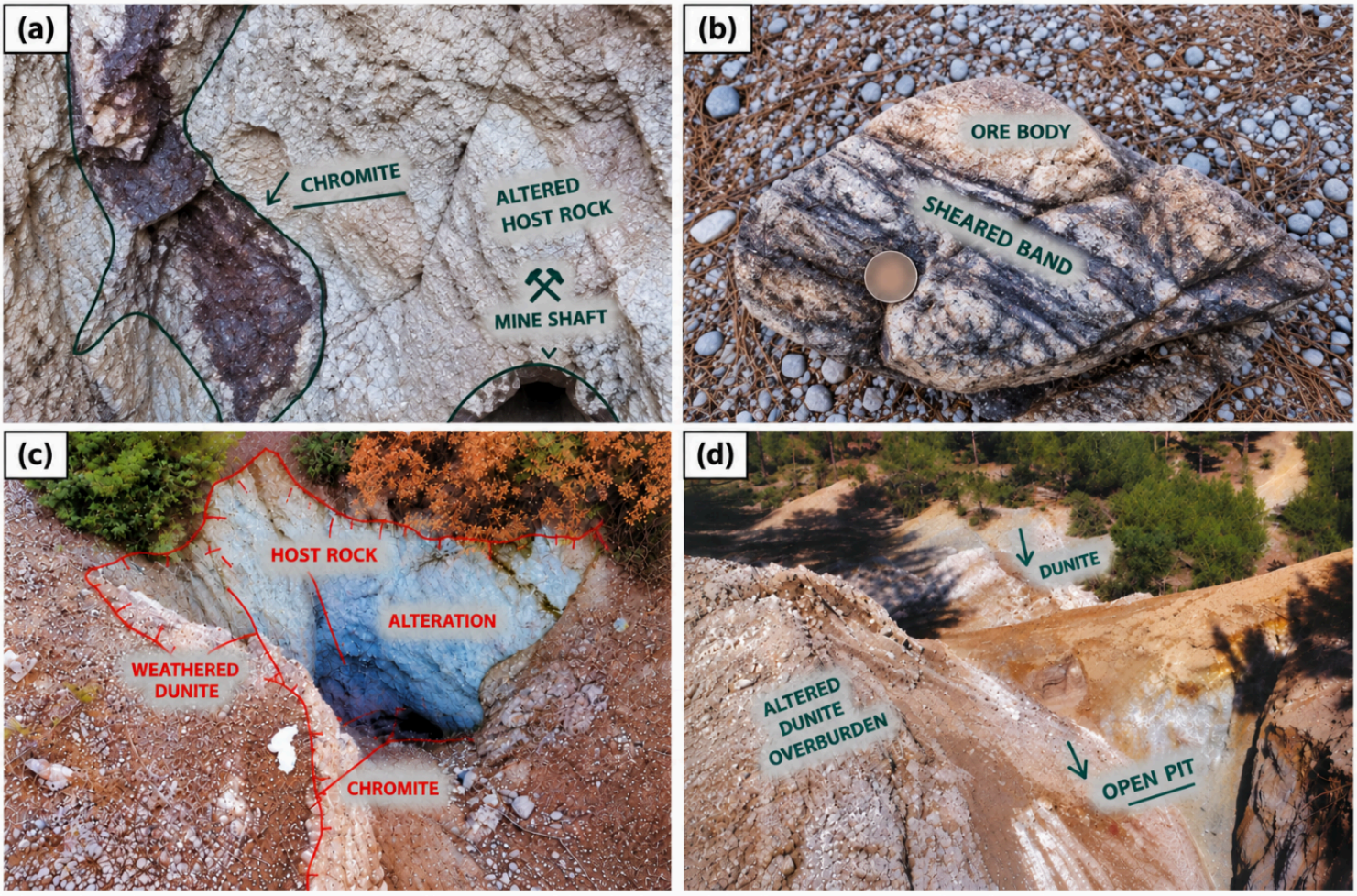


Figure 6

Representative field views of chromite mineralization and former workings, including mineralized zones, banded chromite and altered host rocks.

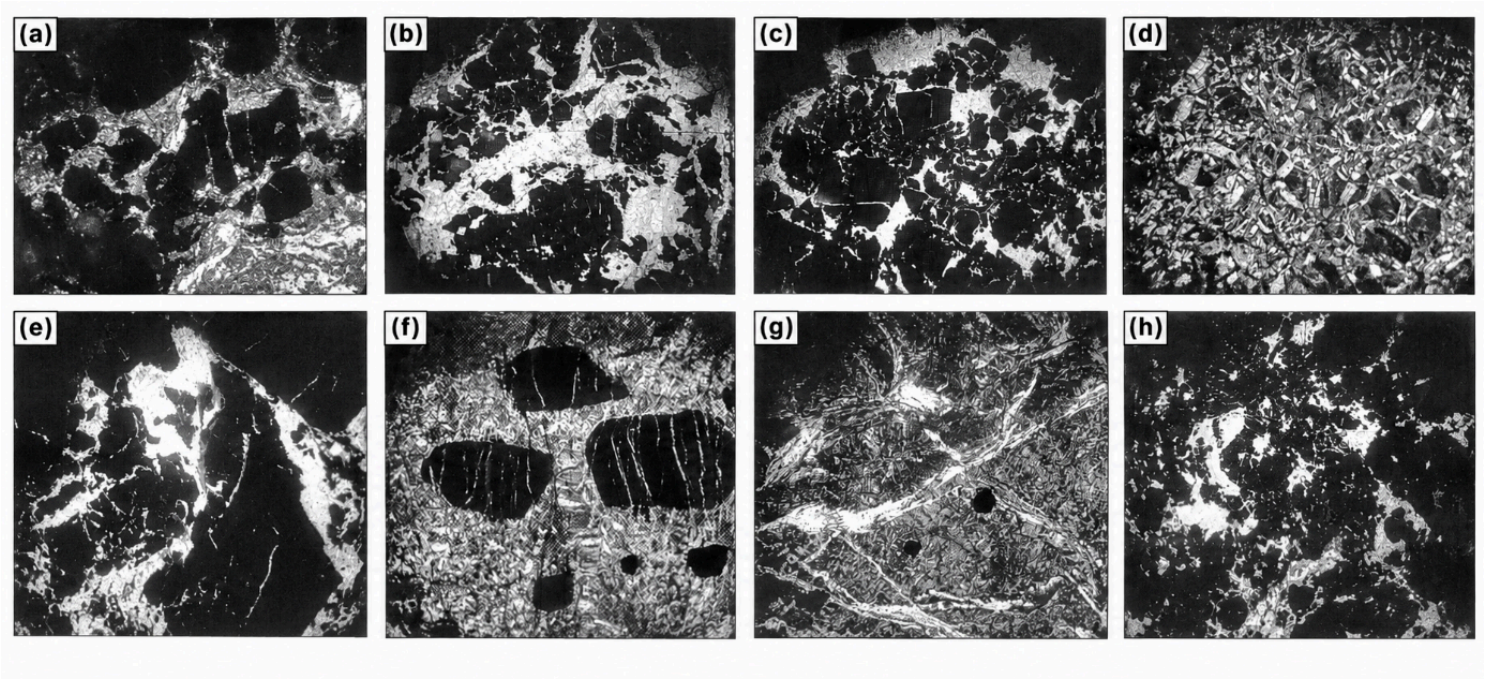


Figure 7

Petrographic features of chromite-bearing rocks. (a) Fragmented chromite in a deformed, oriented serpentine-rich fabric; (b) cataclastic chromite with secondary calcite and albite; (c) chromite-rich cataclastic texture with serpentine and talc; (d) brecciated chromite with secondary carbonate and serpentine. Image width: 3.5 mm.

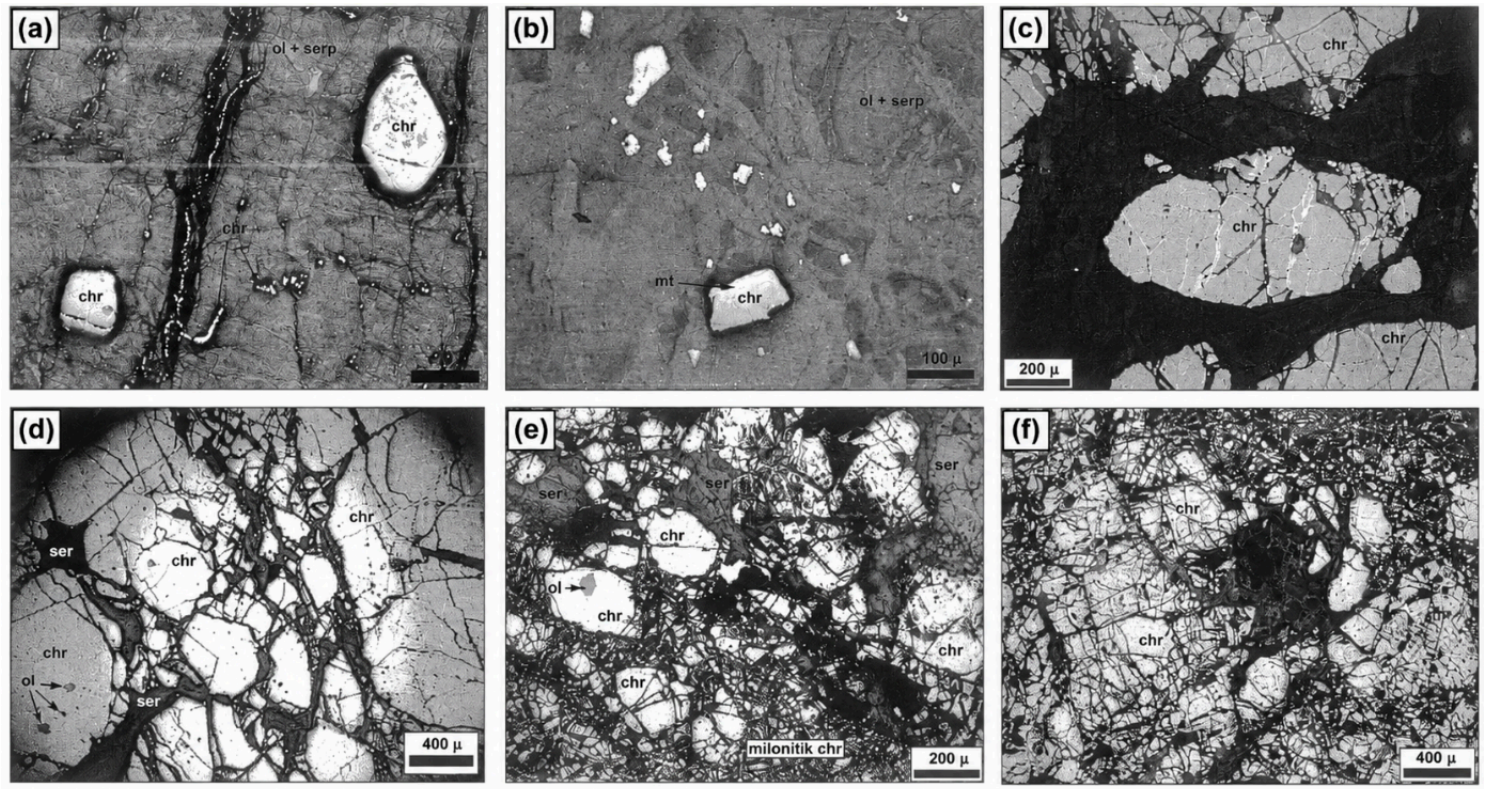


Figure 8

Ore-microscopic characteristics of selected chromite ores. (a) Fragmented and crushed/mylonitic chromite; (b) coarse fractured and brecciated chromite; (c) rim-like texture described as magnetitization in the source record; (d) strongly fractured and locally crushed/mylonitized chromite.

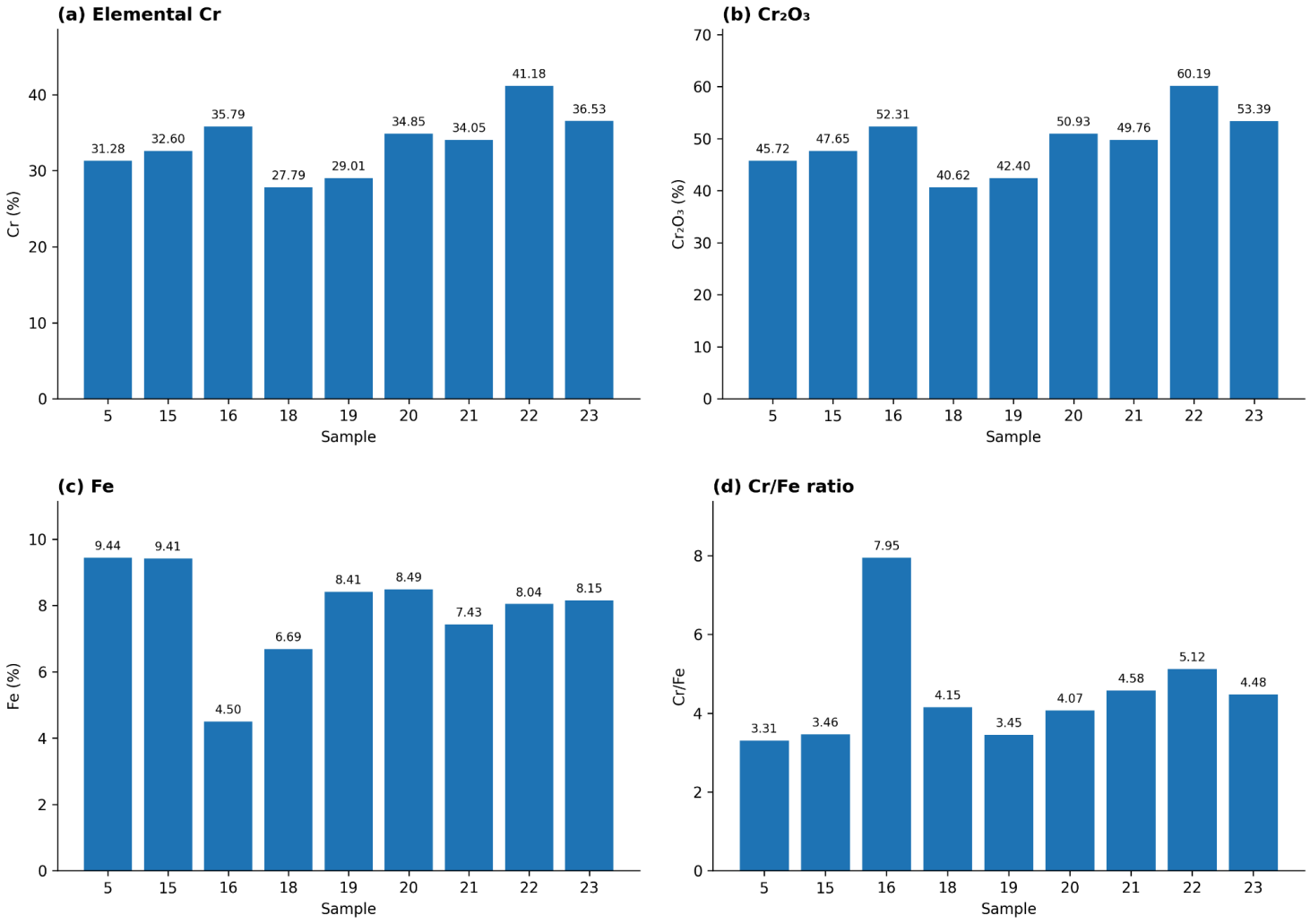


Figure 9

Geochemical characteristics of the chromite ores: (a) elemental Cr; (b) Cr_2O_3; (c) Fe; and (d) reported Cr/Fe ratios.

Supplementary Files

This is a list of supplementary files associated with this preprint. Click to download.

- SupplementaryInformation.docx